Economics Working Paper Series

2016 - 10

The Role of El Niño Southern Oscillation in Commodity Price Movement and Predictability

David Ubilava

June 13, 2016

The Role of El Niño Southern Oscillation in Commodity Price Movement and Predictability

David Ubilava*

School of Economics, University of Sydney

This Draft:† June 13, 2016

Abstract

How are commodity prices related to the El Niño Southern Oscillation (ENSO) cycle, and has this relationship altered over time? Despite overwhelming evidence suggesting an important role played by the ENSO in global commodity production, the relationship between this climate anomaly and prices is not a trivial corollary, and requires careful investigation. To account for potentially complex dynamics in the ENSO–price relationship, this study applies a time–varying smooth transition autoregressive (TV–STAR) modeling framework to monthly series of the sea surface temperature anomalies in the *Niño3.4* region and 46 primary commodity prices spanning the January 1982 – December 2015 period. The findings suggest apparent linkages between ENSO shocks and a set of agricultural commodities, as well as forestry commodities and metals. An unexpected deviation in ENSO results in two-to-five percentage point change in prices, while up to 30 percent of price variation in the selected commodities can be attributed to ENSO shocks in the intermediate and long run. Importantly, there are benefits to regime–dependent modeling, which in some instances facilitates unveiling causal linkages that may have been camouflaged in a linear setting. Several commodity prices also reveal evidence of structural change, and in those instances, the ENSO effect appears to have been mitigated over time, suggesting some adaptive response to the known economic consequences of this climate anomaly.

Keywords: Commodity Prices, El Niño Southern Oscillation, Nonlinear Dynamics, Structural Change, Time–Varying Smooth Transition Autoregression

JEL Codes: C51, E31, Q54

*E-Mail: david.ubilava@sydney.edu.au

†This paper has benefited from valuable comments of seminar participants at CREATES, University of Illinois, University of Minnesota, Tbilisi State University, University of Pretoria, University of Adelaide, University of New South Wales, and the 25th New Zealand Econometric Study Group Meeting. An earlier version the manuscript was circulated under the title *"Rises and Falls in Primary Commodity Prices: Blame it on ENSO or Leave Them Kids Alone?"* From the earlier version to the current, there are important changes in research execution and results. The author acknowledges financial support from the Faculty of Arts and Social Sciences, through the Research Support and Incubator Schemes. The findings and the views expressed in this paper are solely those of the author.

1 Introduction

In the wake of arguably one of the strongest El Niño occurrences in recent history, news concerning anticipated global food shortage and subsequent commodity price spikes have headlined popular media and intensified academic discussions (e.g., Carlson, 2015; Craymer, 2015; Meng and Hsiang, 2015). The concern is not unfounded, as some of the most devastating weather events – such as droughts, hurricanes, and tsunamis – have been historically associated with deviations in the El Niño Southern Oscillation (ENSO) cycle (Pielke Jr and Landsea, 1999). The ENSO cycle features El Niño – and its counterpart, La Niña – as extreme phases. These anomalous deviations of the considered climate phenomenon are assessed more scrupulously now than ever, plausibly as a result of their improved predictability (e.g., Ludescher et al., 2014), and due to a better general understanding of their global economic consequences (e.g., Cashin et al., 2015). While the effect of ENSO shocks on world commodity production is well–evidenced in the literature (e.g., Handler and Handler, 1983; Iizumi et al., 2014), nontrivial linkages between this climate anomaly and a broad range of primary commodity prices remain to be better understood. In that respect, this study aims to address two important questions: (i) what are the consequences of ENSO shocks on dynamic behavior of commodity prices? and (ii) has the ENSO–price relationship changed over the course of recent history?

The question of the potential linkages between the ENSO anomalies and commodity prices primarily stems from a causal mechanism involving the production effect of this climate phenomenon. ENSO anomalies can largely dictate weather conditions in many parts of the world (e.g., Ropelewski and Halpert, 1987; Stone et al., 1996; Barlow et al., 2001), increasing probabilities of droughts or floods, as illustrated in Figure 1. Several features of the ENSO effect – also documented in the literature – are notable. First, not only tangent to the Pacific (where ENSO occurs), but also distant regions are impacted, owing to the presence of the so called *teleconnections*, which radiate the ENSO impulses around the globe (Rasmusson, 1991; Stone et al., 1996). Second, regions within the tropical band are affected more than other regions (see, also, Hsiang and Meng, 2015). Third, the weather effects of the two counterpart anomalies are not exactly the mirror images of each other (e.g., Hoerling et al., 1997; Zhang et al., 2014).

The observed climatology can have implications for the ENSO–price relationship, and the way this relationship is modeled. First of all, many primary commodities are produced in the areas that are directly affected by ENSO anomalies. If the weather effects are synchronized due to ENSO – e.g., simultaneous droughts in different regions during the El Niño event – the global price effect is likely to be amplified. Alternatively, if there are offsetting weather effects in different commodity producing regions, the global price effect of ENSO shocks may be mitigated, despite its apparent effect on production in specific geographic areas. In addition, asymmetries in the weather effect of ENSO may also manifest into asymmetries in price responses to ENSO shocks. That is, for example, La Niña shocks may not necessarily result in price decrease even if El Niño shocks cause price increase of a particular commodity.

Modeling asymmetries in commodity price responses to ENSO shocks is at core of the current analysis. There are reasons to believe that ENSO effect on price dynamics may be nonlinear. First, as noted above, it is likely that one extreme – e.g., El Niño – can disturb market conditions in different ways, as compared to its counterpart – La Niña. If so, price dynamics during the two extreme regimes may be different, i.e., asymmetric. Moreover, economic agents may react differently to news related to one or the other extreme events (for example, El Niño is a better known and more "talked about" anomaly of the two). Second, it is reasonable to assume, that small deviations in ENSO may have an effect that is disproportional to its large deviations. That is, observed weather patterns associated with ENSO events are likely to be more apparent during the most extreme episodes of this climate anomaly. As noted above, economic agents are more likely to react to news suggesting strong El Niño or La Niña, as compared to their moderate manifestations.

The foregoing discussion suggests that there may be several regimes of commodity price dynamics, and switches between these regimes may be conditioned on the status of ENSO. Moreover, these switches may be gradual – rather than instantaneous – because of heterogeneity among economic agents who likely face different transaction costs, or possess different ability or willingness to process ENSO–related information. So, there may be a continuum of thresholds at which a switch between regimes happens. Thus, a generalized version of a threshold model – capable of capturing smooth transition between the regimes – is a framework that will be suitable in the current analysis.

In addition to the regime–dependent nonlinearities, the question of structural change in the ENSO–price relationship has gained relevance in accord with an improved overall understanding of this climate anomaly and its economic consequences. There are at least two reasons that could have facilitated potentially evolving dynamics between these two variables. First, the increasingly improved knowledge of the phenomenon may be resulting in a different reaction from economic agents now than before. Second, factors other than ENSO (e.g., technological change, policy effect, etc.), have changed dynamics of primary commodity prices during past several decades (Enders and Holt, 2012), which may have altered causal linkages between ENSO and prices as well. Whatever may be the cause, it is vital to account for parameter non-constancy in the regression setting, to facilitate accurate identification of the relationship between ENSO and commodity prices. Moreover, the aforementioned structural change is likely to be gradual, rather than abrupt, given the nature of technological change and adaptation.

To address potential parameter non-constancies, and regime–dependent nonlinearities in the ENSO–price relationship, this study adopts a time–varying smooth transition autoregressive (TV–STAR) model (e.g., Lundbergh et al., 2003). A TV–STAR can be seen as a generalized framework that nests an array of different nonlinear models, as well as a basic linear autoregression, as special cases. Because an exact nature of the ENSO–price relationship is *a priori* unknown, and moreover given that these relationships are likely to vary across different commodity groups, the aforementioned flexibility afforded by the TV–STAR framework is a particularly attractive feature of the modeling exercise. It is worth noting that the TV–STAR platform has already been successfully applied to analyze commodity price behavior Holt and Craig (2006); Balagtas and Holt (2009); Hood and Dorfman (2015), albeit in different contexts.

This study offers several contributions to the literature. First, this research incorporates a comprehensive set of individual spot prices to gain insights of the ENSO effect across different commodity categories. Second, this study addresses nonlinearities and structural change in the ENSO–commodity price relationship in a TV–STAR framework, thus, allowing for possibility of regime–dependent behavior in commodity price dynamics, where regimes can be a nonlinear function of time or ENSO anomalies. In so doing, this research sets up a modeling framework that

can be extended as a forecasting exercise, to examine nonlinear Granger causality in a potentially changing environment (e.g., Pesaran and Timmermann, 2004; Giacomini and Rossi, 2010). In addition, this study applies well–established and newly introduced methods – such as the generalized impulse response functions of Koop et al. (1996), and the generalized forecast error variance decomposition of Lanne and Nyberg (2016) – to illustrate the role of ENSO in commodity price dynamics and their variability, particularly due to nonlinear modeling.

2 Nonlinear Modeling and Testing

The econometric framework of the current analysis is designed to account for possible structural change and regime–dependent nonlinearities in the commodity price dynamics, particularly in response to ENSO shocks. While there may be several options for nonlinear modeling, a conveniently fitting approach for the current analysis is the TV–STAR modeling framework. The concept of smooth transition regressions was pioneered by Bacon and Watts (1971). Subsequently, Chan and Tong (1986) were first to introduce its time series variant – the smooth *threshold* autoregressive model, which later became popular under the smooth *transition* autoregressive label, or simply STAR. In a series of papers, Luukkonen et al. (1988); Teräsvirta and Anderson (1992); Teräsvirta (1994); Eitrheim and Teräsvirta (1996) conceptualized the formal modeling and testing frameworks of the STAR model.

STAR models, and their variations, quickly gained popularity, and have been widely applied to examine asymmetric dynamics in macroeconomic variables (e.g., Teräsvirta, 1995; Sarantis, 1999; Skalin and Teräsvirta, 2002). More recently, this modeling framework has been applied to investigate nonlinear features of agricultural production and prices (e.g., Craig and Holt, 2008; Balagtas and Holt, 2009), climate variables, including ENSO (Hall et al., 2001; Ubilava and Helmers, 2013), and their effect commodity prices (Ubilava, 2012; Ubilava and Holt, 2013). Despite this popularity, a brief description of the econometric specification and the testing framework of the STAR–type models is in order.

2.1 A Smooth Transition Autoregressive Model

Consider an additive nonlinear (i.e., piecewise linear) univariate time series model:

$$y_t = \boldsymbol{\phi}_0' \boldsymbol{w}_t + \sum_{k=1}^{K-1} \boldsymbol{\phi}_k' \boldsymbol{w}_t G_k \left(s_{k,t}; \boldsymbol{\theta}_k \right) + \varepsilon_t, \qquad t = 1, \ldots, T, \tag{1}$$

where y_t is the realization of the dependent variable at time t; $\boldsymbol{w}_t = (1, y_{t-1}, \ldots, y_{t-p})'$ is the vector of explanatory variables, where p is the autoregressive order; $\boldsymbol{\phi}_k = (\phi_{k0}, \phi_{k1}, \ldots, \phi_{kp})'$, $k = 0, \ldots, K-1$, are the vectors of associated parameters, where K denotes the total number of regimes in the model. In addition, the vector of explanatory variables, $\boldsymbol{w}_t$, may also include a set of deterministic or exogenous variables, but we omit those now for the sake of brevity. $G_k \left(s_{k,t}; \boldsymbol{\theta}_k \right)$ is a transition function, by construction bounded between 0 and 1, where $s_{k,t}$ is the transition variable, and $\boldsymbol{\theta}_k$ is the set of parameters associated with (and defining the type or the curvature of) the transition function (as discussed below). Finally, $\varepsilon_t \sim iid(0, \sigma_\varepsilon^2)$ is the white noise process.

A set of restrictions can transform equation (1) to well–known autoregressive models. For example, if $G_k \left(s_{k,t}; \boldsymbol{\theta}_k \right) = 0$, $\forall k$, equation (1) becomes a basic linear autoregression:

$$y_t = \boldsymbol{\phi}' \boldsymbol{w}_t + \varepsilon_t. \tag{2}$$

If $K = 2$ and $G \left(s_t; \boldsymbol{\theta} \right) = \{0, 1\}$, i.e., the transition function is an indicator function, equation (1) becomes a threshold autoregression (TAR) of Tong and Lim (1980) and Tsay (1989).

Alternatively, if $K = 2$ and $G \left(s_t; \boldsymbol{\theta} \right) \in [0, 1]$, i.e., the transition function takes on a continuum of values between 0 and 1, equation (1) becomes a smooth transition autoregression (STAR) of Luukkonen et al. (1988) and Teräsvirta (1994):

$$y_t = \boldsymbol{\phi}_0' \boldsymbol{w}_t + \boldsymbol{\phi}_1' \boldsymbol{w}_t G \left(s_t; \gamma, c \right) + \varepsilon_t, \tag{3}$$

where $G \left(s_t; \gamma, c \right)$ can take several possible forms. Two commonly applied transition functions are

logistic and *exponential* – respectively forming the LSTAR and ESTAR models – given by:

$$G^{(l)}(s_t;\gamma,c)=\left\{1+\exp\left[\gamma\left(\frac{s_t-c}{\sigma_s}\right)\right]\right\}^{-1} \tag{4}$$

$$G^{(e)}(s_t;\gamma,c)=\left\{1-\exp\left[\gamma\left(\frac{s_t-c}{\sigma_s}\right)^2\right]\right\} \tag{5}$$

In these smooth transition functions, the parameter vector consists of the smoothness parameter $\gamma>0$, and the centrality parameter, c, the latter usually constrained by $[\kappa_{s_t},1-\kappa_{s_t}]$, where κ_{s_t} is the truncation factor, usually set to the 15th percentile of the transition variable.

A practical benefit of working with STAR models is that they embed previously defined AR and TAR models as the special cases. For example, the LSTAR converges to the linear AR model when $\gamma\to 0$, and to the TAR model when $\gamma\to\infty$. Furthermore, if the transition variable is set to be a function of time, e.g., $t^*=t/T$, equation (3) will turn into a time–varying autoregression.

Finally, if $K=3$, that is, if a model contains two transition functions, of which one is a function of time, then we have a TV–STAR model as follows:

$$y_t=\boldsymbol{\phi}_0'\boldsymbol{w}_t+\boldsymbol{\phi}_1'\boldsymbol{w}_tG(s_t;\gamma_c,c)+\boldsymbol{\phi}_2'\boldsymbol{w}_tG(t^*;\gamma_\tau,\tau)+\varepsilon_t, \tag{6}$$

where, similar to c, $\tau\in[\kappa_{t^*},1-\kappa_{t^*}]$; the rest are as defined above.

2.2 Testing Linearity and Parameter Constancy in Smooth Transition Models

The question of whether a time–varying or a regime–dependent nonlinearity is truly an underlying feature of the data, is a testable hypothesis. The adequate hypothesis, i.e., $H_0:\gamma=0$, cannot be examined directly, however, due to unidentified nuisance parameters (Davies, 1977, 1987) in the nonlinear model specification. To illustrate the point, consider a two–regime STAR model as in equation (3), where $s_t=y_{t-d}$, $0<d\leq p$. It can be reduced to a linear AR model either by imposing a restriction on the transition parameter, i.e. $\gamma=0$, or by imposing a restriction on the autoregressive parameters associated with the additive regime of the model, i.e. $\phi_{11}=\phi_{12}=\ldots=\phi_{1p}=0$. The standard test statistics, therefore, are no longer applicable. But the issue can be circumvented by approximating the transition function about $\gamma=0$, using a third order Taylor

series expansion (Luukkonen et al., 1988; Teräsvirta, 1994, for details, see). The result is a testable auxiliary regression:

$$y_t = \varphi_0 + \sum_{j=0}^{3} \boldsymbol{\varphi}_j' \boldsymbol{v}_t s_t^j + \xi_t, \tag{7}$$

where $\boldsymbol{v}_t = (y_{t-1}, \ldots, y_{t-p})'$, $\boldsymbol{\varphi}_j = (\varphi_{j1}, \ldots, \varphi_{jp})'$, and ξ_t combines the original error term, ε_t, and the approximation error resulting from the Taylor series expansion. The linearity test is now equivalent to testing the null hypothesis of H_0': $\varphi_{ij} = 0$, $\forall\ i = 1, \ldots, 3$, $j = 1, \ldots p$. Additionally, tests against LSTAR and ESTAR models are also embedded in the testing framework. In particular, H_{03}': $\varphi_{3j} = 0$ and H_{01}': $\varphi_{1j} = 0 \mid \varphi_{kj} = 0$, $\forall\ k = 2, 3$; $j = 1, \ldots, p$, are tests against LSTAR; while H_{02}': $\varphi_{2j} = 0 \mid \varphi_{3j} = 0$, $j = 1, \ldots, p$, is a test against ESTAR. The suitable model is selected based on probability values of the above hypotheses (e.g., Teräsvirta, 1994).

Several features, associated with the nonlinear model selection, need to be noted. First, the transition variable, s_t, is often *a priori* unknown. In such instances, a set of candidate transition variables are considered, and the most appropriate one is selected based on probability values associated with the null hypothesis of linearity. In conjunction with the aforementioned, one may also estimate several candidate models, and decide on the suitable transition variable and the type of nonlinear function based on the model fit (e.g., Akaike Information Criterion), as well as the remaining nonlinearity test results. Second, the parameter constancy test is a special case of the linearity test, where s_t is substituted by t^* in equation (7). Typically, parameter nonconstancy is addressed, i.e., a TVAR is estimated where applicable, before moving on to testing and estimating a STAR or a TV–STAR. Finally, if a TV–STAR is a suspect, the so called *specific–to–general* approach can be implemented, which involves estimating the multiple–regime model (e.g., van Dijk and Franses, 1999), where both time–varying and regime–dependent components are incorporated as transition functions (see, for example, Lundbergh et al., 2003; Holt and Craig, 2006).

3 Data

This study uses monthly series of the ENSO index and the primary commodity prices spanning the period from January 1982 to December 2015. Two better known indices depicting ENSO

cycles are the pressure-based Southern Oscillation Index (SOI), and the sea-surface temperature (SST) measure. Different previous studies have used either or both of these indices (e.g., Brunner, 2002; Ubilava and Holt, 2013; Cashin et al., 2015), but the measure of SST anomalies derived from the observations collected in the *Niño 3.4* region – a rectangular area between $5°\text{N} - 5°\text{S}$ and $170°\text{W} - 120°\text{W}$ in the equatorial Pacific – has become increasingly more common in the climatology literature. So, this study will also apply this anomaly, which is a monthly deviation from the average historic measure in that month during the 1981 – 2010 base period, and is tabulated by the Climate Prediction Center at the National Oceanic and Atmospheric Administration. A positive deviation, i.e., an unusual warming of the SST, is indicative of the El Niño phase, while a negative deviation, i.e., an unusual cooling of the SST, points to the La Niña episode. From here forward, the term *ENSO* will be used interchangeably and synonymously to the sea surface temperature anomaly in the *Niño 3.4* region.

Primary commodity price series are collected from the World Bank and the International Monetary Fund publications. These are spot prices (FOB or CIF), and are indicative of world prices of the commodities. This study considers several important commodity groups, which includes grains and cereals, forestry, farms and fishery, vegetable oils and meals, and industrial and rare metals. See Table 1 for the complete list and a brief description of commodities used in this study. For the purposes of the analysis, these nominal sport prices are deflated using the U.S. producer price index (PPI), collected from the U.S. Bureau of Labor, and then transformed to natural logarithms. From here forward, *prices* will refer the natural logarithm of real commodity prices, unless otherwise stated.

4 Model Selection and Estimation

The building block of most nonlinear models, and certainly the ones considered in this study, is a basic linear specification. Let y_t denote the $I(1)$ price of a commodity in period t,[1] and let z_t denote the $I(0)$ ENSO measure in the same period.[2] Moreover, similar to Brunner (2002), let ENSO be

[1] The commodity-specific subscript is omitted for simplicity.

[2] The assumptions concerning the degrees of integration are supported by the Augmented Dickey Fuller (ADF) and the Kwiatkowski–Phillips–Schmidt–Shin (KPSS) tests. The test results are available upon request.

weakly exogenous to prices. The following linear regression setting is then a suitable starting point of the analysis:

$$\Delta y_t = \boldsymbol{\alpha}_y(t) + \boldsymbol{\beta}'\boldsymbol{x}_t + \boldsymbol{\theta}'\boldsymbol{z}_t + \varepsilon_t, \tag{8}$$

where $\boldsymbol{\alpha}_y(t)$ is a deterministic component, which is a linear function intercept and seasonal binary variables; $\boldsymbol{x}_t = (y_{t-1}, \Delta y_{t-1}, \ldots, \Delta y_{t-p+1})'$; $\boldsymbol{z}_t = (z_t, z_{t-1}, \ldots, z_{t-q})'$, where p and q are selected using Akaike Information Criterion (AIC), and subject to no serial correlation in ε_t, which is assumed to be white noise, i.e., $\varepsilon_t \sim iid\,(0, \sigma_\varepsilon^2)$; and the rest are parameter vectors to be estimated.

In turn, the ENSO variable is also assumed to follow an autoregressive process:

$$z_t = \boldsymbol{\alpha}_z(t) + \boldsymbol{\eta}'\boldsymbol{z}_{t-1} + \nu_t, \tag{9}$$

where $\boldsymbol{\alpha}_z(t)$ is a deterministic component as before; $\boldsymbol{z}_{t-1} = (z_{t-1}, \ldots, z_{t-r})'$, where again, r is selected based on AIC, and subject to no serial correlation, so that $\nu_t \sim iid\,(0, \sigma_\nu^2)$; and the rest are as defined above.

Once the linear models, as specified in equations (8) and (9), are identified, we turn to linearity and parameter constancy testing, using the auxiliary regression framework outlined in Section 2, and letting $s_t = z_{t-d}$, where $1 \leq d \leq r$. In the case of the ENSO equation, the model is assumed to be nonlinear in all of its components. Thus, if the null of linearity is rejected, the following STAR variant of equation (9) is estimated:

$$z_t = \boldsymbol{\alpha}_{z0}(t) + \boldsymbol{\eta}_0'\boldsymbol{z}_{t-1} + \left[\boldsymbol{\alpha}_{z1}(t) + \boldsymbol{\eta}_1'\boldsymbol{z}_{t-1}\right] G(s_t; \gamma_c, c) + \nu_t \tag{10}$$

In the case of the price equation, the model is assumed to have a time–varying autoregressive component along with an intercept, and be nonlinear in distributed lags of ENSO. This is a relatively more parsimonious specification of the TV–STAR model, primarily motivated from potential issues associated with identification of the parameters in different regimes. Similar to Enders and Holt (2012), the currently specified time–varying component allows for potentially smooth transition between the regimes due to the structural change, but in addition to shifts in mean, this study also

accounts for changes in short–term dynamics of commodity prices. Also, unlike Ubilava (2012); Ubilava and Holt (2013), the regime–dependent nonlinearity here is conditioned on the state of ENSO, rather than the state (or a linear combination) of lagged prices.

The model selection algorithm proceeds as follows. First, we test the null hypotheses of linearity and parameter constancy based on equation (7). If the null of parameter constancy is rejected, we estimate a time–varying autoregressive (TVAR) model using a nonlinear least squares method, and then test the null of no remaining nonlinearity. If we also reject the null of remaining nonlinearity, we estimate a TV–STAR model. Alternatively, if in the first stage, we fail to reject the null of parameter constancy, but reject the null of linearity, we estimate a STAR model. Given the aforementioned decision tree, we can ultimately identify and estimate one of the four potential models: (i) an autoregressive distributed lag model; (ii) a time–varying autoregressive distributed lag model; (iii) an autoregressive smooth transition distributed lag model; and (iv) a time–varying autoregressive smooth transition distributed lag model, respectively given by equation (8), and the following set of equations:

$$\Delta y_t = \boldsymbol{\alpha}_{y0}(t) + \boldsymbol{\beta}_0' \boldsymbol{y}_{t-1} + \left[\boldsymbol{\alpha}_{y1}(t) + \boldsymbol{\beta}_1' \boldsymbol{y}_{t-1}\right] G(t^*; \gamma_\tau, \tau) + \boldsymbol{\theta}' \boldsymbol{z}_t + \varepsilon_t \tag{11}$$

$$\Delta y_t = \boldsymbol{\alpha}_{y0}(t) + \boldsymbol{\beta}_0' \boldsymbol{y}_{t-1} + \boldsymbol{\theta}_0' \boldsymbol{z}_t + \boldsymbol{\theta}_1' \boldsymbol{z}_t G(s_t; \gamma_c, c) + \varepsilon_t \tag{12}$$

$$\Delta y_t = \boldsymbol{\alpha}_{y0}(t) + \boldsymbol{\beta}_0' \boldsymbol{y}_{t-1} + \left[\boldsymbol{\alpha}_{y1}(t) + \boldsymbol{\beta}_1' \boldsymbol{y}_{t-1}\right] G(t^*; \gamma_\tau, \tau) + \boldsymbol{\theta}_0' \boldsymbol{z}_t + \boldsymbol{\theta}_1' \boldsymbol{z}_t G(s_t; \gamma_c, c) + \varepsilon_t, \tag{13}$$

where $G(t^*, \gamma_\tau, \tau)$ and $G(s_t, \gamma_c, c)$ respectively are logistic functions of $t^* = t/T$ and $s_t = z_{t-d}$, where the delay factor, $d \leq q$, is a non-negative integer; the rest are as defined before.

5 The Estimation Results, Interpretation, and Discussion

To summarize, in 20 out of the considered 46 price series there is evidence of causal linkages with ENSO. That is, a contemporaneous or lagged realizations of the ENSO variable belong to the commodity price equation, as suggested by the AIC. Such a relationship, in some instances, is better identified when the regime–dependent nonlinearity in the ENSO effect is accounted for. In particular, in eight of the price equations a nonlinear specification appears to facilitate the better

fit of the data. Moreover, in five of the aforementioned 20 price equations with the ENSO variable, and an additional twelve price equations without the ENSO variable on the right-hand-side, we observe a structural change of some sort (i.e., instantaneous or gradual) during the time span in consideration. The price series, and the estimated transition functions of those commodities where ENSO is incorporated in the equation, are featured in Figure 2. In majority of the cases, transition between the regimes appears to be gradual, i.e., the smooth transition modeling seems to be an appropriate nonlinear modeling framework vis-á-vis instantaneous, threshold–like autoregressive models.[3] To better understand the dynamics of the estimated equations we turn to impulse–response analysis.

5.1 Generalized Impulse–Responses and Error Variance Decomposition

The nonlinear model dynamics depend on a set of factors, such as the direction and the intensity of initial shocks, i.e., impulses; the information set prior to these shocks, i.e., histories; and the idiosyncratic disturbances that occur throughout the forecast horizon. This implies that the so called naïve extrapolation – which is applicable in linear models to generate impulse–response functions – will yield biased results, and is not valid in the case of nonlinear models. To circumvent this issue, Koop et al. (1996) proposed a numerical approximation technique that produces the generalized impulse–response functions (GIRs) as follows:

$$\pi_x\left(h, \upsilon_t, \omega_{t-1}\right) = \mathbb{E}\left(x_{t+h}|\upsilon_t, \omega_{t-1}\right) - \mathbb{E}\left(x_{t+h}|\omega_{t-1}\right), \qquad h = 1, 2, \ldots, \tag{14}$$

where $\pi_x\left(h, \upsilon_t, \omega_{t-1}\right)$ is a GIR of a variable x, at a horizon h, and where $\omega_{t-1} \in \Omega_{t-1}$ denotes a point in time with initial conditions from the set of histories under consideration, and $\upsilon_t \in \Upsilon_t$ denotes an impulse, i.e., the realization of an initial shock, from the distribution of shocks under consideration; finally, $\mathbb{E}$ is an expectation operator. Assuming that υ_t, ω_{t-1} and $\{x_t\}$ are realizations from the same stochastic process, $\pi_x\left(h, \upsilon_t, \omega_{t-1}\right)$ itself – which is the difference between two random variables

[3] The estimated smoothness and location parameters, along with their standard errors, are not presented here, but are available upon request.

– represents a realization of the random variable (Koop et al., 1996), given by:

$$\pi_x\left(h, \Upsilon_t, \Omega_{t-1}\right) = \mathbb{E}\left(x_{t+h}|\Upsilon_t, \Omega_{t-1}\right) - \mathbb{E}\left(x_{t+h}|\Omega_{t-1}\right), \tag{15}$$

The aforementioned framework of the generalized impulse–response analysis lends itself naturally to the recently proposed generalized forecast error variance decomposition (GFEVD) of Lanne and Nyberg (2016). This method, in essence, generalizes the approach put forward by Pesaran and Shin (1998), and augments it to a nonlinear multivariate framework. In particular, a realization of the GFEVD at horizon h, for a given history ω_{t-1}, is given by:

$$\lambda^k_{ij,\omega_{t-1}} = \frac{\sum_{h=0}^{k} \pi_i\left(h, \upsilon_{jt}, \omega_{t-1}\right)^2}{\sum_{h=0}^{k} \pi_i\left(h, \upsilon_{1t}, \omega_{t-1}\right)^2 + \sum_{h=0}^{k} \pi_i\left(h, \upsilon_{2t}, \omega_{t-1}\right)^2}, \tag{16}$$

where j and i denote impulse and response variables, and the rest are as defined above. Thus, by construction, $\lambda^k_{ij,\omega_{t-1}} \geq 0$, and $\sum_j \lambda^k_{ij,\omega_{t-1}} = 1$. As such, $\lambda^k_{ij,\omega_{t-1}}$ represents a relative impact of variable j in relation to the cumulative impact of all variables in consideration. Similar to $\pi_x\left(h, \upsilon_t, \omega_{t-1}\right)$, $\lambda^h_{ij,\omega_{t-1}}$ is also realization of a random variable, conditioned on histories and shocks. In practice, $\lambda^h_{ij,\omega_{t-1}}$ are integrated across histories and shocks to obtain the GFEVDs. See Lanne and Nyberg (2016) for details of the GFEVD computation.

5.2 Bootstrap Resampling and Scenarios for the Impulse–Response Analysis

In principle, Ω_{t-1} can contain every history from the available index set, but a subset of histories, $\Omega'_{t-1} \subseteq \Omega_{t-1}$, is often applied to obtain conditional expectations. For example, if we are interested in price dynamics during the El Niño conditions, only the histories associated with this phase are sampled. Or, if we are interested in price dynamics after a structural change, only the histories associated with the most recent regime of the index set are sampled.

This study considers a total of five scenarios. First, to illustrate the overall effect, a sample of histories is randomly selected from the available index set. Further, to compare dynamics between the two extreme ENSO regimes, subsets of histories are sampled from periods associated with El Niño or La Niña conditions only. Finally, to visualize dynamics before and after the structural

change, histories are randomly sampled from the respective periods of the index set. In each given scenario, a bootstrap resampling algorithm is applied first to the ENSO equation, and subsequently to the price equation, to obtain the GIRs. Shocks, or impulses, are drawn from the distribution of residuals from the ENSO equation. In particular, a total of 80 shocks, exceeding one standard deviation of residuals from the ENSO equation, are randomly sampled (with replacement). To assess sign–specific asymmetries, both positive and negative ENSO shocks are considered. That is, absolute values of the sampled impulses are respectively added to or subtracted from the realization of ENSO at the zero horizon. Finally, 200 vectors of idiosyncratic surprises are randomly sampled (with replacement) from the estimated ENSO model, where the length of the vector is set to 24 (i.e., two years). Thus, for each history–shock combination, 200 bootstrap extrapolates are generated with and without an initial shock. These bootstrap extrapolates are then averaged at each horizon, yielding conditional expectations, with and without an initial shock, as in the right-hand-side of equation (14), yielding the GIR of ENSO. The aforementioned conditional expectations of ENSO are subsequently incorporated in the price equation, where as previously, 200 bootstrap price extrapolates are generated using idiosyncratic surprises that are randomly sampled (with replacement) from the estimated price equation. So, a total of 4,800 history–shock specific GIRs are obtained by taking a difference between the conditional expectations of prices, with and without the ENSO shocks, yielding the distribution of GIRs across histories and shocks for positive and negative ENSO shocks, and each scenario considered. Note that prices are modeled as first-differences, so as the final step, obtained GIRs are integrated to recover the effect of the ENSO shocks on log levels of real commodity prices.

Figure 3 illustrates the median, and the 5th and 95th percentiles of the calculated GIRs based on randomly sampled histories (unconditional on time period or the ENSO regime). Several features of interest are revealed from this analysis. On many occasions, the ENSO shocks appear to have long-term impact on commodity prices. This is primarily due to persistence in prices, as the ENSO shock itself tends to dissolve in approximately a one–year period. Moreover, different commodity groups are affected differently by ENSO shocks, both in terms of the magnitude and the direction of the effect. Finally, in several commodities, asymmetries are apparent, that is, the impulse responses

due to El Niño and La Niña shocks of equivalent magnitude are not mirror images of each other.

To better illustrate the regime–dependent asymmetries we turn to GIRs generated from subsets of histories associated with El Niño or La Niña conditions only. The resulted GIRs are illustrated in Figure 4. First of all, the difference in ENSO dynamics between the two regimes is notable. The ENSO tends to oscillate but dissolve relatively soon after the shocks during the El Niño regime, but is characterized by a more persistent behavior during the La Niña regime. As for the commodities, aluminum prices respond to ENSO shocks during El Niño conditions but not otherwise. On the other hand, cocoa prices respond to ENSO shocks during La Niña phase only. Prices of hard logs and sunflower-seed oils also – which did not respond statistically significantly when histories were not conditioned on ENSO regimes – appear to be impacted by ENSO shocks when history–specific nonlinearities are accounted for.

The foregoing GIRs do not account for the observed structural change in a number of commodities. That is, histories are randomly sampled from the index set, which includes time periods before and after the structural change. To examine differences in commodity price dynamics due to the structural change, we sample the first 60 histories of the available index set – i.e., the period before a structural change – and the last 60 histories of the index set – i.e., the period after a structural change. The resulted GIRs are illustrated in Figure 5. In all three commodities, the effect of ENSO shocks appear to be less amplified and tend to dissolve after the structural change, in comparison with the larger in magnitude and more persistent effect observed prior to the structural change. Such finding points to a possible ongoing adaptation with respect to the effect of ENSO phenomenon. For example, it might be that fishmeal consumers adjust their inventories in anticipation of El Niño, thus mitigating the long–run effect of its repercussions.

5.3 The Topology of Commodity Price Responses to ENSO Shocks

Agricultural commodities, expectedly, belong to a key category, prices of which are most affected by ENSO. Within this category, prices of vegetable oils are most responsive to surprises in this climate phenomenon. On average, an unanticipated positive shock to ENSO, i.e., an El Niño–like event, results in up to five percentage point increase in prices of major vegetable oils, such as

palm oil and soybean oil. The effect is particularly apparent after the subsequent one–year period. Sunflower-seed oil prices behave similarly, although the effect is only apparent during the El Niño conditions. Approximately 15 percent of the vegetable oil price variation after a one–year period, and up to a third of the price variation after a two–year period, can be attributed to ENSO shocks, as suggested by GFEVDs featured in Table 3.

Fishmeal prices increase by up to three percent, and salmon prices increase by approximately two percent, following an El Niño shock – an observation that is hardly controversial, given the supply–side effect of this climate anomaly. Notably, prices of a close substitute to fishmeal – soybean meal – decrease by approximately two percent after an El Niño shock, which manifests into an amplified fishmeal–to–soybean meal price ratio dynamics in response to ENSO shocks (Ubilava, 2014). Beef prices, on the other hand, decrease after El Niño, although this change is only of a half of a percentage point in magnitude.

Among the considered grains and cereals, wheat prices increase by two percentage points after a negative ENSO shock, i.e., a La Niña–like event. This effect is consistent with an expectation, as the two largest wheat exporters – U.S. and Canada – tend to experience droughts during La Niña episodes. Soybean prices, on the other hand, reveal curious dynamics in response to ENSO shocks. Initially, they resemble a pattern similar to wheat prices, i.e., up to one percent decrease in prices during first year following an El Niño shock, but subsequently, perhaps due to vertical price transmission stemming from the vegetable oil market, the effect reverts, resulting in up to one percent price increase starting approximately one year after the shock. Up to 25 percent of wheat price variation, but only 10–15 percent of soybean price variation, can be attributed to ENSO during the one–to–two year period after the shock. Notably, prices of other cereals, e.g., barley, maize, and sorghum, do not reveal evidence of causal linkages with ENSO. This finding points to the mitigating effect of regional diversification of crop production, suggesting that losses in one set of regions are offset by gains in another set of regions.

This study considers two varieties of coffee: the *Robusta* coffee, which is typically produced in Southeast Asia, and the *Arabica* coffee, which is predominantly harvested in Central and South American countries. Findings suggest that only the Arabica variety responds statistically signifi-

cantly to ENSO shocks. In particular, a La Niña shock appears to result in more than two percent increase in Arabica coffee prices. This finding is in accord with evidence that the price spread of the two coffee varieties tends to widen after La Niña episodes. Approximately 15 percent of Arabica coffee price variation can be attributed to ENSO shocks.

Forestry is another category of commodities prices of which appear to be affected by ENSO shocks. Prices of soft logs increase by approximately one percent after an El Niño shock. Price dynamics of hard logs, in turn, reveal a clear regime–dependency. During El Niño conditions, an unexpected El Niño shock results in an approximately two percent increase in prices. Alternatively, during La Niña conditions, prices of hard logs initially increase by more than one percent after a La Niña shock, but subsequently decrease by up to two percent. In terms of variance decomposition, approximately 15–25 percent of price variation of these commodities can be attributed to ENSO shocks during the one–to–two year horizon.

A number of metal prices also respond to ENSO shocks, and in a number of cases the effect is of the regime–dependent nature. For example, prices of aluminum increase by approximately three percent after an El Niño shock, but this effect is evident during the El Niño conditions only. Prices of tin also increase by almost two percent in the intermediate–run following an El Niño shock during the El Niño conditions. On the other hand, prices of tin increase by more than two percent following a La Niña shock during the La Niña conditions. Twenty–to–thirty percent of these metal price variation at the one–to–two year horizon can be attributed to ENSO shocks. Notably, the ENSO effect on gold prices, while statistically insignificant is not economically meaningful. For example, following El Niño, gold prices appear to increase statistically significantly by approximately a tenth of a percentage point.

6 Conclusion

Literature on commodity price behavior is not thin. Thus far, there is a fair bit of consensus on some of the well–established characteristic features of commodity prices. For example, commodity price series are found to be highly persistent (Cashin et al., 2000; Ghoshray, 2013), with occasional spikes, and possibly nonlinear dynamics (Tomek, 2000; Cashin et al., 2002; Enders and Holt, 2012).

Even so, the question about "why prices move as they do?" is still lingering among economists. This study is an attempt to address the aforementioned question by examining the extent to which an exogenous climatic factor – the El Niño Southern Oscillation – is causing the primary commodity price movement. In so doing, this study builds upon and contributes to the previous research in two main directions. First, it investigates the relationship between ENSO and an extensive list of primary commodity prices. Second, this study allows and accounts for the possibility of a structural change and the ENSO–related nonlinearities in commodity price dynamics.

Findings of this research suggest that ENSO plays an economically important and statistically significant role in price behavior of an array of commodities, and this effect extends beyond the anticipated agricultural sector. Much of the effect is likely supply driven, be that due to shortage of water for irrigation of field crops, or hydro-energy generation for its use in mining sector. Vegetable oils and protein meals represent the key group of commodities that respond to ENSO shocks – the finding that is consistent with several previous studies (Brunner, 2002; Laosuthi and Selover, 2007; Ubilava and Holt, 2013). Among other affected food and agricultural commodities are wheat, soybeans, beef, salmon, and coffee. Forestry commodities as well as metals are also impacted by ENSO shocks, and the effect is particularly apparent when nonlinearities are accounted for. The effect of an ENSO surprise, which is measured as the 0.3°C deviation in the SST on average, results in one–to–five percent change in commodity prices, which also translates to 15–30 percent price variation attributable to ENSO shocks in the intermediate run.

Findings of this study are largely in agreement with previous research, but also add considerable knowledge to the existing literature. In a number of the considered cases, the time–varying regime-dependent modelling facilitates the identification of the causal linkages between ENSO and prices, which appear to be camouflaged in a linear setting. In that respect, results of this study have important policy implications, suggesting that care is needed to avoid possible faulty conclusions due to linear modelling, if the relationship is, in fact, nonlinear. In addition, these findings carry important welfare implications, especially for developing nations, as their exports, terms of trade, and the economic growth have historically relied on primary commodities (Deaton, 1999; Chinn and Coibion, 2014). This can be an important research direction motivated by this analysis.

References

Bacon, D. and D. Watts (1971). Estimating the Transition between Two Intersecting Straight Lines. *Biometrika 58*(3), 525–534.

Balagtas, J. V. and M. T. Holt (2009). The Commodity Terms of Trade, Unit Roots, and Nonlinear Alternatives: A Smooth Transition Approach. *American Journal of Agricultural Economics 91*(1), 87–105.

Barlow, M., S. Nigam, and E. Berbery (2001). ENSO, Pacific Decadal Variability, and US Summertime Precipitation, Drought, and Stream Flow. *Journal of Climate 14*(9), 2105–2128.

Brunner, A. (2002). El Nino and World Primary Commodity Prices: Warm Water or Hot Air? *Review of Economics and Statistics 84*(1), 176–183.

Carlson, D. (2015). El Niño Takes Toll on US Rice Farmers Ű And Points to Even Higher Prices. *The Guardian*.

Cashin, P., H. Liang, and C. J. McDermott (2000). How Persistent Are Shocks to World Commodity Prices? *IMF Staff Papers 42*(2), 177–217.

Cashin, P., C. J. McDermott, and A. Scott (2002). Booms and Slumps in World Commodity Prices. *Journal of Development Economics 69*(1), 277–296.

Cashin, P. A., K. Mohaddes, and M. Raissi (2015). Fair Weather or Foul? The Macroeconomic Effects of El Niño. Globalization and Monetary Policy Institute Working Paper No. 239.

Chan, K. and H. Tong (1986). On Estimating Thresholds in Autoregressive Models. *Journal of Time Series Analysis 7*(3), 179–190.

Chinn, M. D. and O. Coibion (2014). The Predictive Content of Commodity Futures. *Journal of Futures Markets 34*(7), 607–636.

Craig, L. A. and M. T. Holt (2008). Mechanical Refrigeration, Seasonality, and the Hog-Corn Cycle in the United States: 1870-1940. *Explorations in Economic History 45*(1), 30–50.

Craymer, L. (2015). El Niño Tests How Soft Commodities Weather the Storm. *The Wall Street Journal*.

Davies, R. (1977). Hypothesis Testing when a Nuisance Parameter is Present only under the Alternative. *Biometrika 64*(2), 247–254.

Davies, R. (1987). Hypothesis Testing when a Nuisance Parameter is Present only under the Alternative. *Biometrika 74*(1), 33–43.

Deaton, A. (1999). Commodity Prices and Growth in Africa. *The Journal of Economic Perspectives 13*(3), 23–40.

Eitrheim, O. and T. Teräsvirta (1996). Testing the Adequacy of Smooth Transition Autoregressive Models. *Journal of Econometrics 74*(1), 59–75.

Enders, W. and M. T. Holt (2012). Sharp Breaks or Smooth Shifts? An Investigation of the Evolution of Primary Commodity Prices. *American Journal of Agricultural Economics 94*(3), 659–673.

Ghoshray, A. (2013). Dynamic Persistence of Primary Commodity Prices. *American Journal of Agricultural Economics 95*(1), 153–164.

Giacomini, R. and B. Rossi (2010). Forecast Comparisons in Unstable Environments. *Journal of Applied Econometrics 25*(4), 595–620.

Hall, A., J. Skalin, and T. Teräsvirta (2001). A Nonlinear Time Series Model of El Niño. *Environmental Modelling & Software 16*(2), 139–146.

Handler, P. and E. Handler (1983). Climatic Anomalies in the Tropical Pacific Ocean and Corn Yields in the United States. *Science 220*(4602), 1155–1156.

Hoerling, M. P., A. Kumar, and M. Zhong (1997). El Niño, La Niña, and the Nonlinearity of Their Teleconnections. *Journal of Climate 10*(8), 1769–1786.

Holt, M. T. and L. A. Craig (2006). Nonlinear Dynamics and Structural Change in the U.S. Hog-Corn Cycle: A Time-Varying STAR Approach. *American Journal of Agricultural Economics 88*(1), 215–233.

Hood, H. B. and J. H. Dorfman (2015). Examining Dynamically Changing Timber Market Linkages. *American Journal of Agricultural Economics 97*(5), 1451–1463.

Hsiang, S. M. and K. C. Meng (2015). Tropical Economics. *American Economic Review: Papers & Proceedings 105*(5), 257–261.

Iizumi, T., J.-J. Luo, A. J. Challinor, G. Sakurai, M. Yokozawa, H. Sakuma, M. E. Brown, and T. Yamagata (2014). Impacts of El Niño Southern Oscillation on the Global Yields of Major Crops. *Nature Communications 5*(3712).

Koop, G., M. Pesaran, and S. Potter (1996). Impulse Response Analysis in Nonlinear Multivariate Models. *Journal of Econometrics 74*(1), 119–147.

Lanne, M. and H. Nyberg (2016). Generalized Forecast Error Variance Decomposition for Linear and Nonlinear Multivariate Models. *Oxford Bulletin of Economics and Statistics*.

Laosuthi, T. and D. D. Selover (2007). Does El Niño Affect Business Cycles? *Eastern Economic Journal 33*(1), 21–42.

Ludescher, J., A. Gozolchiani, M. I. Bogachev, A. Bunde, S. Havlin, and H. J. Schellnhuber (2014). Very Early Warning of Next El Niño. *Proceedings of the National Academy of Sciences 111*(6), 2064–2066.

Lundbergh, S., T. Teräsvirta, and D. Van Dijk (2003). Time-Varying Smooth Transition Autoregressive Models. *Journal of Business & Economic Statistics 21*(1), 104–122.

Luukkonen, R., P. Saikkonen, and T. Teräsvirta (1988). Testing Linearity Against Smooth Transition Autoregressive Models. *Biometrika 75*(3), 491–499.

Meng, K. and S. Hsiang (2015). El Niño: A Global Weather Event That May Save California – And Destroy the Tropics. *The Guardian*.

Pesaran, H. and Y. Shin (1998). Generalized Impulse Response Analysis in Linear Multivariate Models. *Economics Letters 58*(1), 17 – 29.

Pesaran, M. and A. Timmermann (2004). How Costly is it to Ignore Breaks when Forecasting the Direction of a Time Series? *International Journal of Forecasting 20*(3), 411 – 425.

Pielke Jr, R. and C. Landsea (1999). La Niña, El Niño, and Atlantic Hurricane Damages in the United States. *Bulletin of the American Meteorological Society 80*(10), 2027–2034.

Rasmusson, E. (1991). *Teleconnections Linking Worldwide Climate Anomalies*, Chapter Observational Aspects of ENSO Cycle Teleconnections, pp. 309–343. Cambridge University Press, New York.

Ropelewski, C. and M. Halpert (1987). Global and Regional Scale Precipitation Patterns Associated with the El Niño/Southern Oscillation. *Monthly Weather Review 115*(8), 1606–1626.

Sarantis, N. (1999). Modeling Non-linearities in Real Effective Exchange Rates. *Journal of International Money and Finance 18*(1), 27–45.

Skalin, J. and T. Teräsvirta (2002). Modeling Asymmetries and Moving Equilibria in Unemployment Rates. *Macroeconomic Dynamics 6*(2), 202–241.

Stone, R., G. Hammer, and T. Marcussen (1996). Prediction of Global Rainfall Probabilities Using Phases of the Southern Oscillation Index. *Nature 384*(6606), 252–255.

Teräsvirta, T. (1994). Specification, Estimation, and Evaluation of Smooth Transition Autoregressive Models. *Journal of the American Statistical Association 89*(425), 208–218.

Teräsvirta, T. (1995). Modelling Nonlinearity in US Gross National Product 1889–1987. *Empirical Economics 20*(4), 577–597.

Teräsvirta, T. and H. Anderson (1992). Characterizing Nonlinearities in Business Cycles using Smooth Transition Autoregressive Models. *Journal of Applied Econometrics 7*(S1), S119–S136.

Tomek, W. (2000). Commodity Prices Revisited. *Agricultural and Resource Economics Review 29*(2), 125–137.

Tong, H. and K. S. Lim (1980). Threshold Autoregression, Limit Cycles and Cyclical Data. *Journal of the Royal Statistical Society. Series B (Methodological) 42*(3), 245–292.

Tsay, R. (1989). Testing and Modeling Threshold Autoregressive Processes. *Journal of the American Statistical Association 84*(405), 231–240.

Ubilava, D. (2012). El Niño, La Niña, and World Coffee Price Dynamics. *Agricultural Economics 43*(1), 17–26.

Ubilava, D. (2014). El Niño Southern Oscillation and the Fishmeal–Soya Bean Meal Price Ratio: Regime-Dependent Dynamics Revisited. *European Review of Agricultural Economics 41*(4), 583–604.

Ubilava, D. and C. Helmers (2013). Forecasting ENSO with a Smooth Transition Autoregressive Model. *Environmental Modelling & Software 40*(1), 181–190.

Ubilava, D. and M. Holt (2013). El Niño Southern Oscillation and its Effects on World Vegetable Oil Prices: Assessing Asymmetries using Smooth Transition Models. *Australian Journal of Agricultural and Resource Economics 57*(2), 273–297.

van Dijk, D. and P. Franses (1999). Modeling Multiple Regimes in the Business Cycle. *Macroeconomic Dynamics 3*(3), 311–340.

Zhang, T., J. Perlwitz, and M. P. Hoerling (2014). What is Responsible for the Strong Observed Asymmetry in Teleconnections between El Niño and La Niña? *Geophysical Research Letters 41*(3), 1019–1025.

Tables

Table 1: Description and Origin of the Considered Commodity Prices

Commodity	Notation	Description and Origin
Aluminum	ALM	99.5% minimum purity, LME spot price, CIF UK ports
Arabicas (coffee)	ARB	International Coffee Organization New York cash price, ex-dock New York, (c/lb)
Beef	BEF	Australian and New Zealand 85% lean fores, CIF U.S. import price, (c/lb)
Bananas	BNN	Central America and Ecuador, FOB U.S. ports
Barley	BRL	Canadian No.1 Western Barley, spot price
Cocoa	CCA	International Cocoa Organization cash price, CIF US and European ports
Coconut Oil	CCN	Philippines/Indonesia, in bulk, CIF Rotterdam
Chicken	CHK	Whole bird spot price, Ready-to-cook, whole, iced, Georgia docks, (c/lb)
Copper	CPP	Grade A cathode, LME spot price, CIF European ports
Copra	CPR	Philippines/Indonesia, in bulk, CIF NW European ports
Cotton	CTN	Cotton Outlook 'A Index', Middling 1-3/32 inch staple, CIF Liverpool, (c/lb)
Fishmeal	FSH	Peru pellets, 65% Protein, CIF
Gold	GLD	99.5% fine, London afternoon fixing, average of daily rates
Groundnut Oil	GRN	Any origin, CIF Rotterdam
Hides	HID	Heavy native steers, over 53 pounds, wholesale dealer's price, FOB Chicago, (c/lb)
Hard Logs	HRD	Best quality Malaysian Meranti, import price Japan, ($/m^3)
Hard Sawnwood	HSW	Dark Red Meranti, select and better quality, C&F U.K port, ($/m^3)
Lead	LED	99.97% pure, LME spot price, CIF European Ports
Lamb	LMB	Frozen carcass, Smithfield London, (c/lb)
Maize	MZE	U.S. No.2 Yellow, FOB Gulf of Mexico
Nickel	NCK	Melting grade, LME spot price, CIF European ports
Oranges	ORN	Miscellaneous, CIF French import price
Olive Oil	OLV	Extra virgin less than 1% free fatty acid, ex-tanker price U.K.
Palm Oil	PLM	Malaysia/Indonesia, in Bulk, 5% FFA, CIF NW European Ports
Platinum	PLT	99.9% refined, London afternoon fixing
Peanuts (groundnuts)	PNT	40/50 count per ounce, CIF Argentina
Pork	PRK	51-52% lean Hogs, U.S. price (c/lb)
Robustas (coffee)	RBS	International Coffee Organization New York cash price, ex-dock New York, (c/lb)
Rice	RCE	Thailand 5% broken milled white rice, FOB Bangkok
Rapeseed Oil	RPS	Crude, FOB Rotterdam
Soybean Meal	SBM	Argentine 45/46% extraction (after January 1990); U.S. 44%, CIF Rotterdam
Soybeans	SBN	U.S. No.2 Yellow, CIF Rotterdam
Soybean Oil	SBO	Any origin, crude, FOB ex-mill Netherlands
Soft Logs	SFT	Average export price, U.S. for Douglas Fir, ($/m^3)
Sugar	SGR	ISA daily price, raw, FOB and stowed at greater Caribbean Ports ($/kg)
Salmon	SLM	Farm Bred Norwegian Salmon, export price, ($/kg)
Silver	SLV	99.9% refined, London afternoon fixing
Sunflowerseed Oil	SNF	European Union, FOB NW European ports
Sorghum	SRG	U.S. No.2 milo yellow, FOB Gulf ports
Soft Sawnwood	SSW	Average export price, U.S. for Douglas Fir, ($/m^3)
Tobacco	TBC	Any origin, unmanufactured, general import, CIF U.S.
Tea	TEA	Kenya auction price (after July 1998); London auctions, CIF U.K. warehouses, (c/kg)
Tin	TIN	Standard grade, LME spot price
Wheat	WHT	U.S. No.1 Hard Red Winter, Ordinary Protein, FOB Gulf of Mexico
Wool	WOL	Coarse, 23 micron, Australian Wool Exchange spot quote (c/kg)
Zinc	ZNC	High grade 98% pure

Note: the commodity prices are denominated in US$ per metric ton, unless otherwise specified. The series were sourced from the World Bank and the International Monetary Fund online database.

Table 2: Model Selection and Residual Diagnostics

Commodity	p	q	*Model*	d	p_{t^*}	p_{AC}	p_{ARCH}
ALM	6	2	STAR	0	0.260	0.352	0.000
ARB	3	1	AR		0.450	0.594	0.000
BEF	3	2	STAR	1	0.160	0.705	0.586
BNN	5		TVAR		0.009	0.904	0.007
BRL	2		TVAR		0.740	0.214	0.004
CCA	3	0	STAR	0	0.043	0.754	0.226
CCN	5	5	AR		0.150	0.482	0.522
CHK	2		TVAR		0.013	0.718	0.000
CPP	6		AR		0.240	0.392	0.006
CPR	5	5	AR		0.036	0.307	0.833
CTN	4		AR		0.210	0.553	0.000
FSH	6	0	TVAR		0.850	0.879	0.350
GLD	3	0	TVAR		0.260	0.486	0.011
GRN	2		AR		0.250	0.744	0.120
HID	6		TVAR		0.450	0.523	0.058
HRD	6	1	STAR	1	0.710	0.570	0.000
HSW	3		AR		0.280	0.840	0.000
LED	2		TVAR		0.300	0.672	0.000
LMB	2		TVAR		0.170	0.656	0.004
MZE	2		AR		0.520	0.904	0.782
NCK	2	1	STAR	0	0.530	0.244	0.838
OLV	3	1	TV–STAR	1	0.000	0.412	0.000
ORN	6		AR		0.260	0.126	0.056
PLM	5	6	AR		0.400	0.361	0.808
PLT	2		AR		0.260	0.660	0.012
PNT	6		TVAR		0.046	0.358	0.000
PRK	3		AR		0.130	0.608	0.013
RBS	2		AR		0.180	0.313	0.031
RCE	3		AR		0.460	0.970	0.000
RPS	2		TVAR		0.000	0.614	0.000
SBM	4	5	AR		0.430	0.279	0.196
SBN	2	5	AR		0.064	0.663	0.142
SBO	5	6	AR		0.200	0.723	0.246
SFT	2	3	TVAR		0.004	0.784	0.006
SGR	2		AR		0.720	0.251	0.346
SLM	6	0	AR		0.170	0.055	0.001
SLV	6		TVAR		0.270	0.008	0.000
SNF	4	4	STAR	4	0.900	0.241	0.306
SRG	2		AR		0.390	0.838	0.998
SSW	3		TVAR		0.004	0.304	0.000
TBC	5		TVAR		0.320	0.968	0.001
TEA	3		TVAR		0.570	0.425	0.330
TIN	3	3	TV–STAR	3	0.024	0.866	0.535
WHT	2	0	AR		0.540	0.570	0.010
WOL	3		AR		0.260	0.434	0.655
ZNC	2		AR		0.580	0.869	0.550

Note: the column headed with p indicates the autoregressive lag length; the column headed with q indicates the distributed lag length of ENSO (where applicable); the column headed with *Model* indicates the functional form of the estimated model, which can be a simple autoregressive model, a time–varying autoregressive model, an autoregressive distributed lag model, or any of the three nonlinear models given by equations (11) – (13). Moreover, the column headed with d denotes the delay factor of the estimated STAR model (where applicable). Finally, columns headed with p_{t^*}, p_{AC}, and p_{ARCH} denote probability values associated with hypotheses of remaining parameter nonconstancy, residual autocorrelation, and autoregressive conditional heteroskedasticity, respectively.

Table 3: The Relative Contribution of ENSO to the variance of Selected Commodity Prices

Commodity	$h = 1$	$h = 6$	$h = 12$	$h = 24$
ALM	0.10	0.18	0.23	0.24
ARB	0.13	0.16	0.17	0.17
BEF	0.10	0.12	0.13	0.15
CCA	0.06	0.15	0.21	0.27
CCN	0.07	0.06	0.12	0.31
CPR	0.04	0.04	0.09	0.28
FSH	0.06	0.18	0.26	0.31
GLD	0.00	0.02	0.02	0.03
HRD	0.12	0.12	0.19	0.25
NCK	0.12	0.24	0.29	0.33
OLV	0.09	0.14	0.24	0.33
PLM	0.10	0.09	0.19	0.38
SBM	0.09	0.13	0.17	0.17
SBN	0.06	0.09	0.09	0.17
SBO	0.06	0.06	0.14	0.30
SFT	0.07	0.06	0.12	0.18
SLM	0.04	0.10	0.15	0.18
SNF	0.10	0.15	0.27	0.32
TIN	0.09	0.13	0.23	0.31
WHT	0.06	0.16	0.23	0.28

Figures

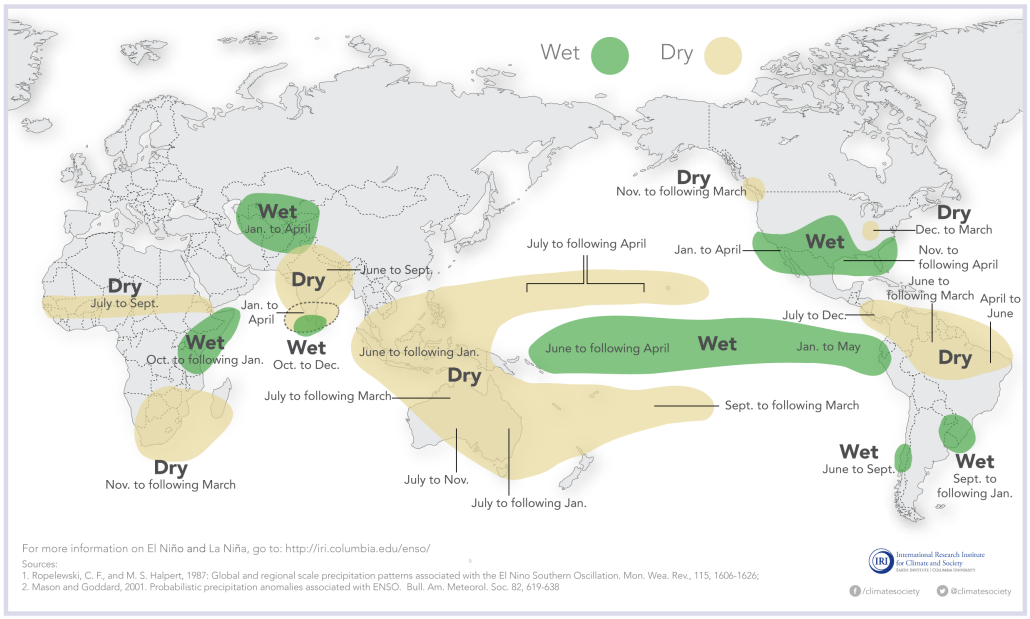

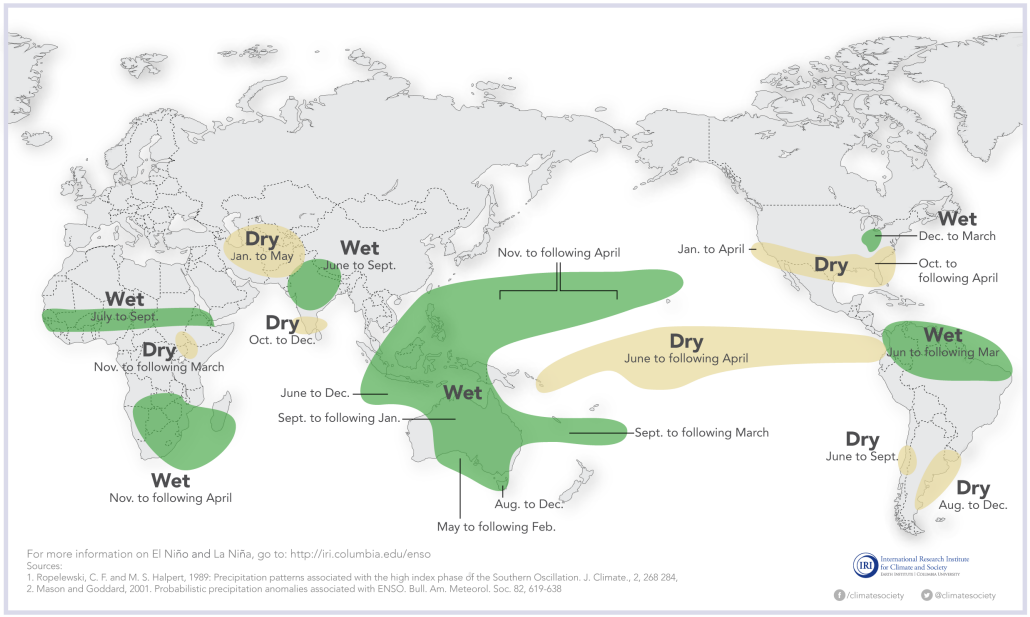

Source: International Research Institute for Climate and Society at Columbia University

Figure 1: Global Weather Effect of ENSO Anomalies

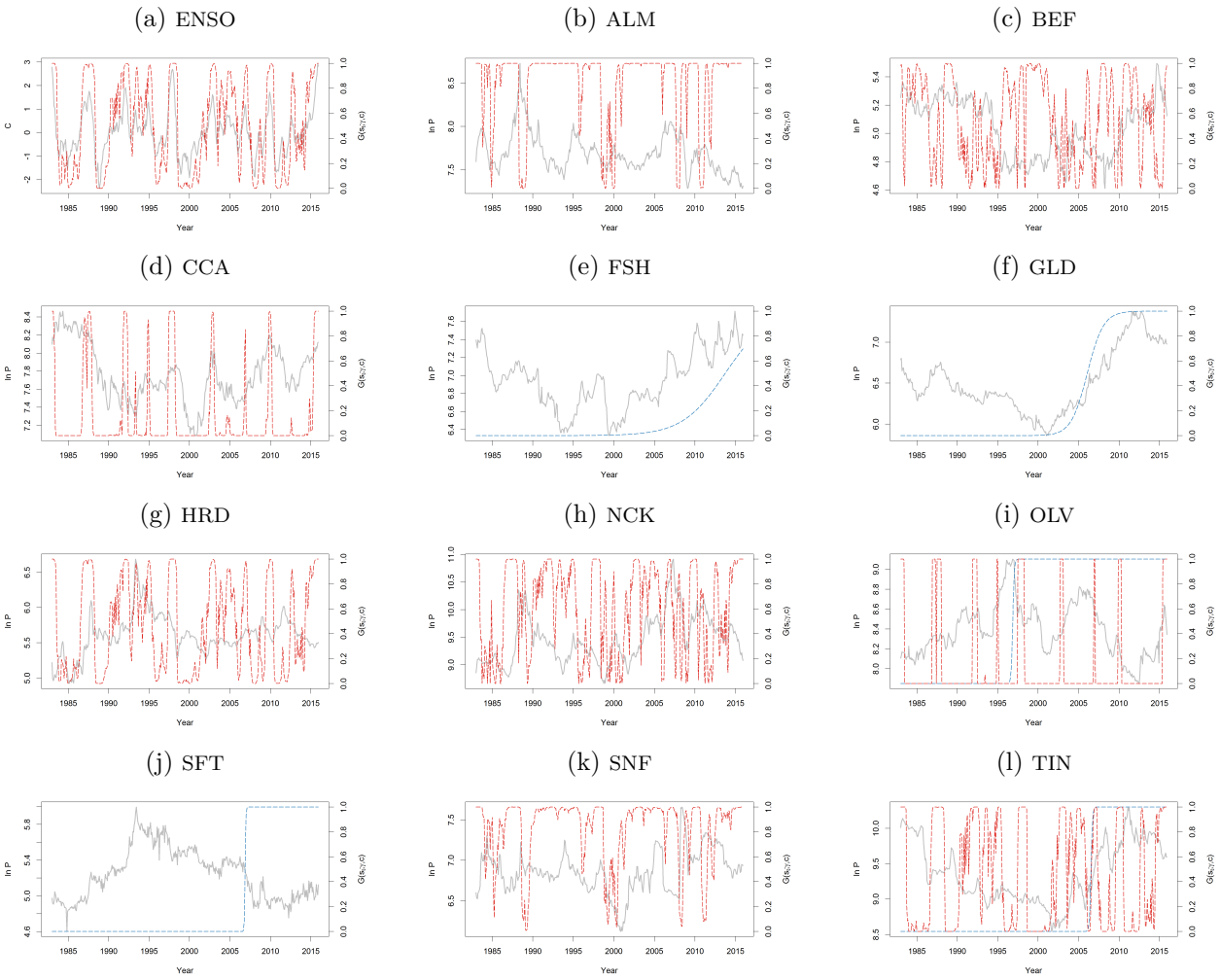

Note: The plots feature time series of the sea surface temperature anomaly and the selected commodity prices (in gray), as well as the transition functions (STAR–type in red and TVAR–type in blue).

Figure 2: Estimated Transition Functions of ENSO and Selected Price Equations

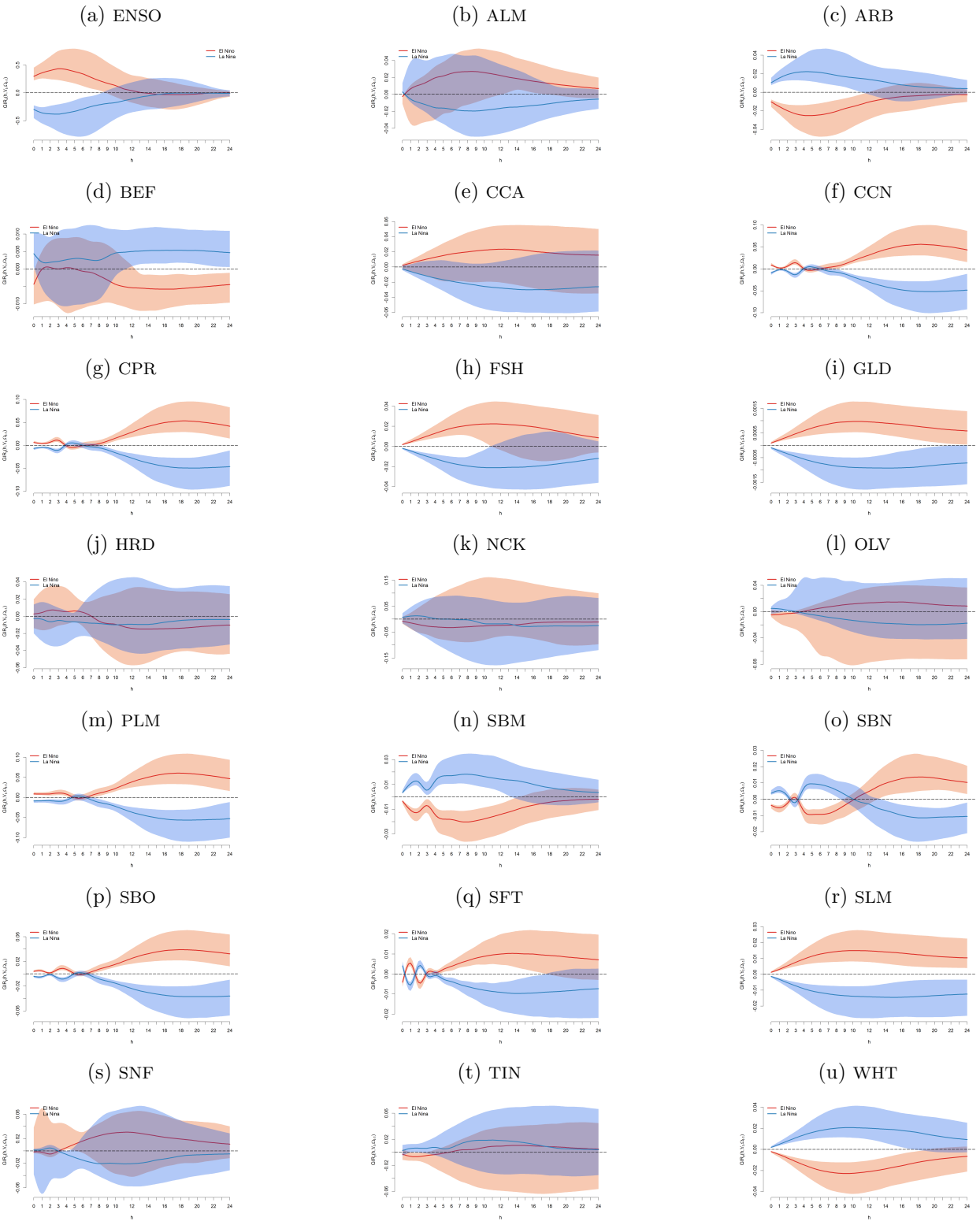

Note: The plots feature the median GIRs (in red or blue for El Niño and La Niña shocks, respectively) and the 90 percent confidence bands (in lighter shades of red and blue) over the 24–month horizon for ENSO and the selected commodity prices.

Figure 3: Generalized Impulse–Response Functions of ENSO and the Selected Commodity Prices

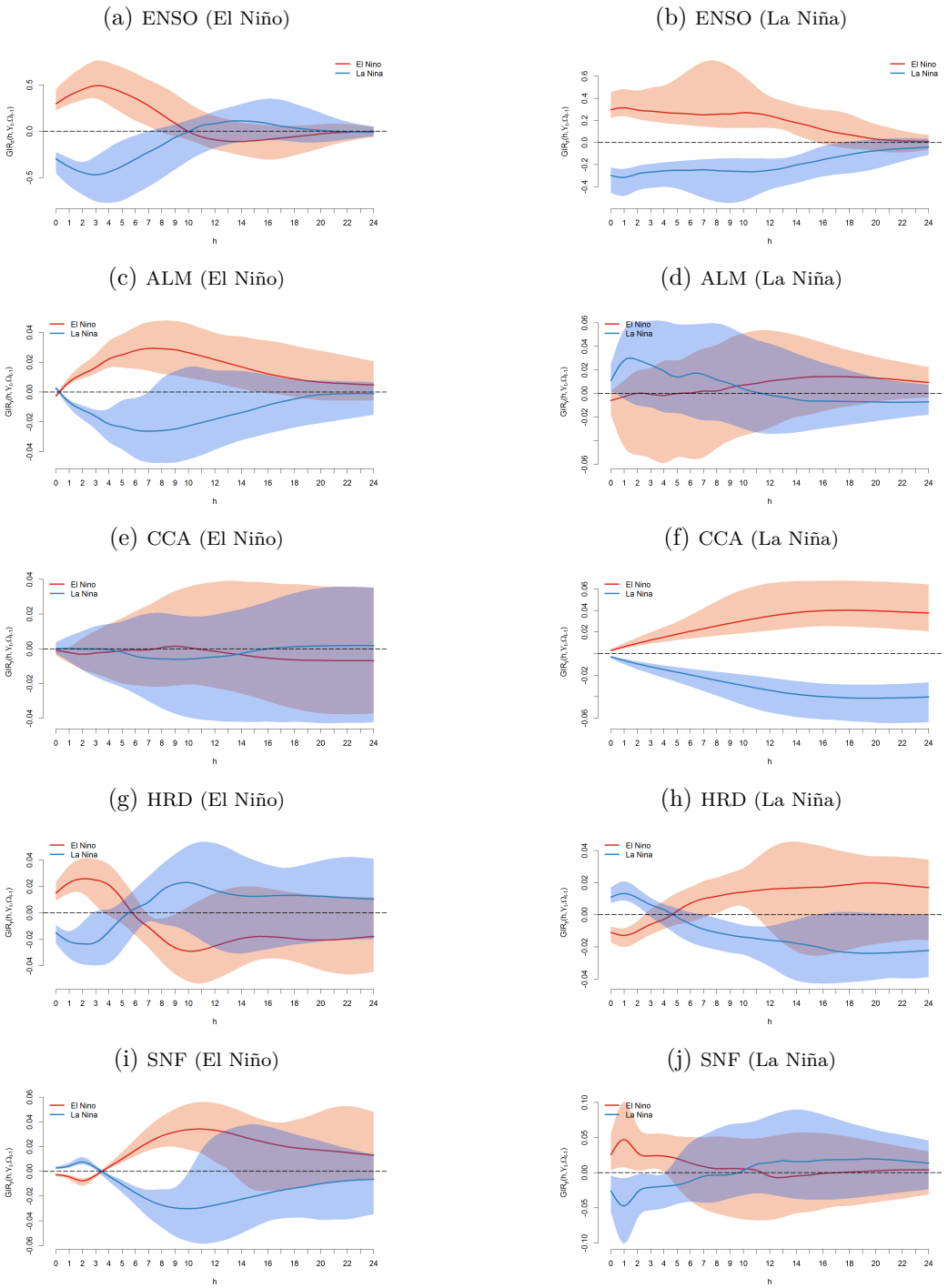

Note: The plots feature the median GIRs (in red or blue for El Niño and La Niña shocks, respectively) and the 90 percent confidence bands (in lighter shades of red and blue) over the 24–month horizon for ENSO and the selected commodity prices.

Figure 4: Regime–Dependent Nonlinearities in ENSO and the Selected Commodity Prices

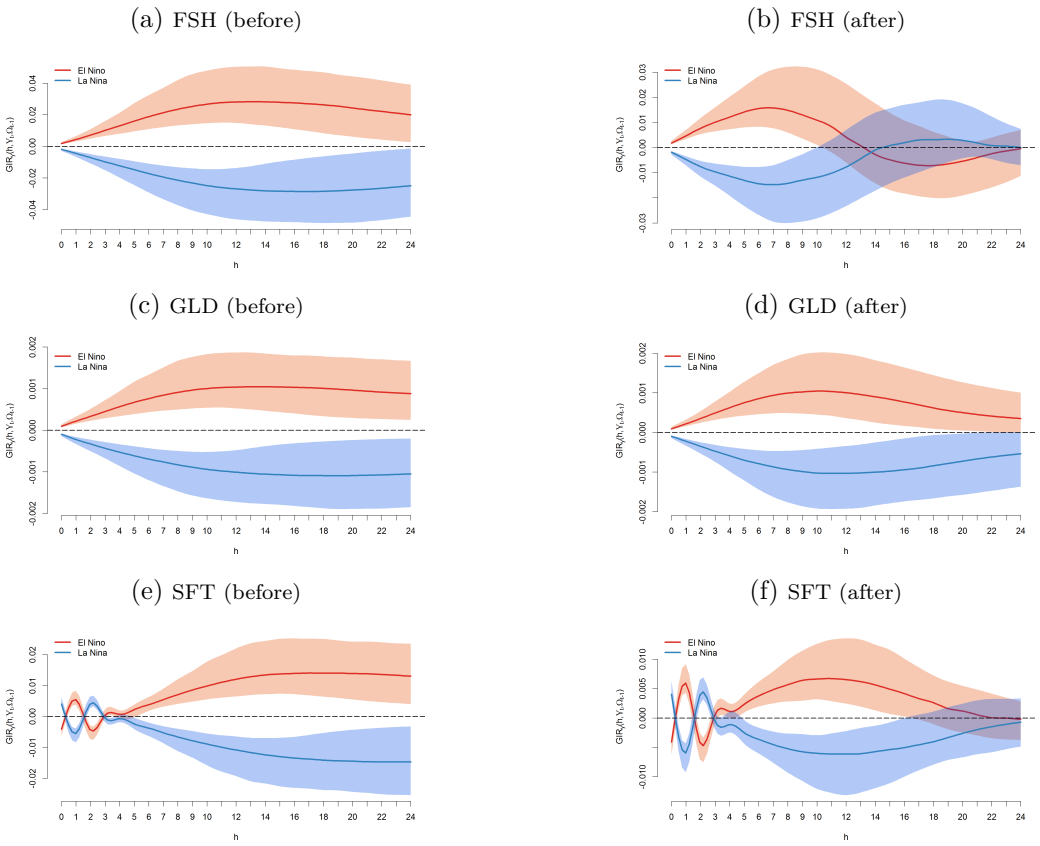

Note: The plots feature the median GIRs (in red or blue for El Niño and La Niña shocks, respectively) and the 90 percent confidence bands (in lighter shades of red and blue) over the 24–month horizon for ENSO and the selected commodity prices.

Figure 5: Structural Change in Fishmeal, Gold, and Soft Log Prices

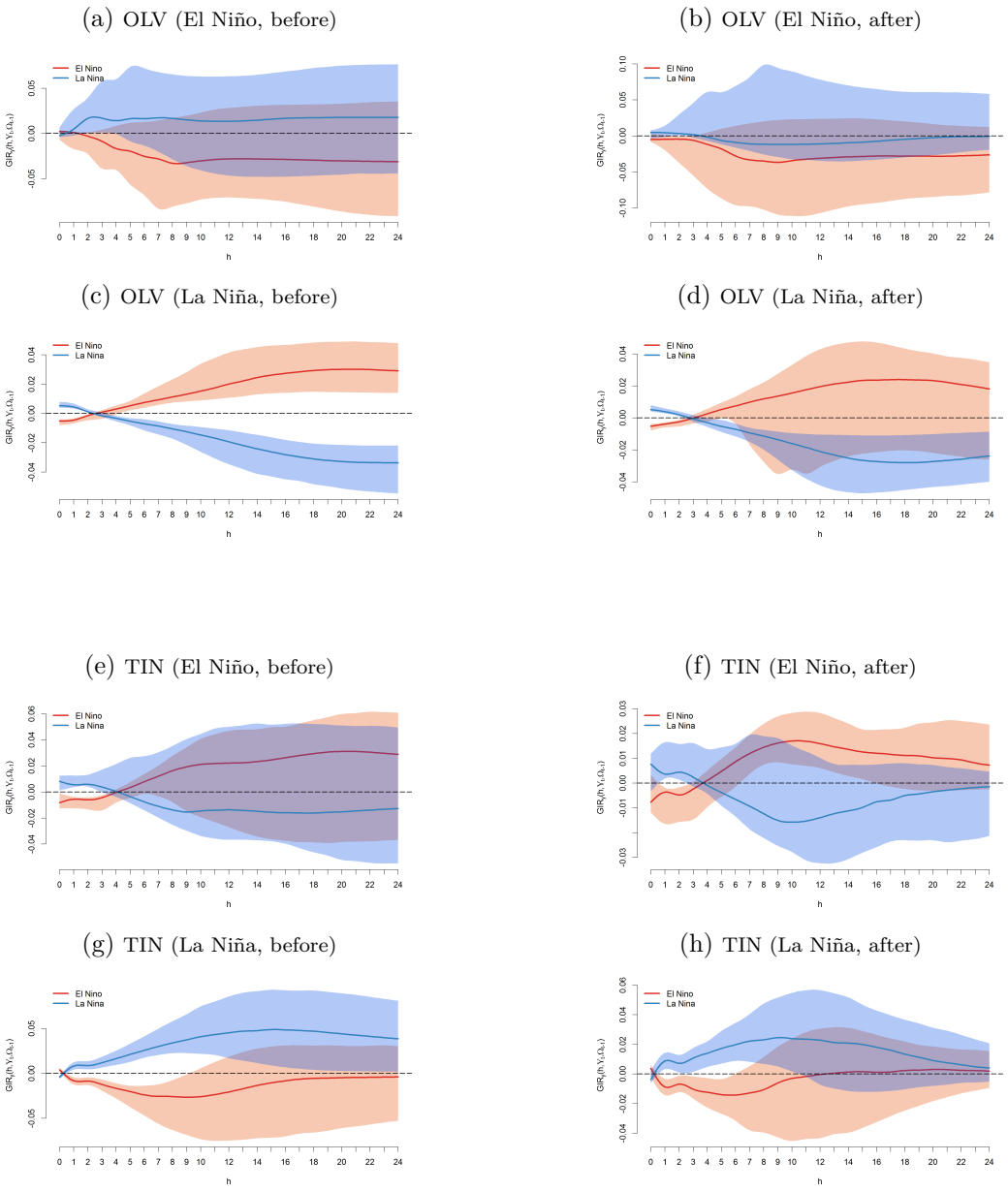

Note: The plots feature the median GIRs (in red or blue for El Niño and La Niña shocks, respectively) and the 90 percent confidence bands (in lighter shades of red and blue) over the 24–month horizon for ENSO and the selected commodity prices.

Figure 6: Structural Change and Regime–Dependent Nonlinearities in Olive Oil and Tin Prices